

Green Chemistry

Accepted Manuscript



This article can be cited before page numbers have been issued, to do this please use: E. Kolobova, E. Pakrieva, S. A.C. Carabineiro, N. Bogdanchikova, A. Kharlanov, S. O. Kazantsev, J. Hemming, P. Mäki-Arvela, A. Pestryakov and D. Murzin, *Green Chem.*, 2019, DOI: 10.1039/C9GC00949C.



This is an Accepted Manuscript, which has been through the Royal Society of Chemistry peer review process and has been accepted for publication.

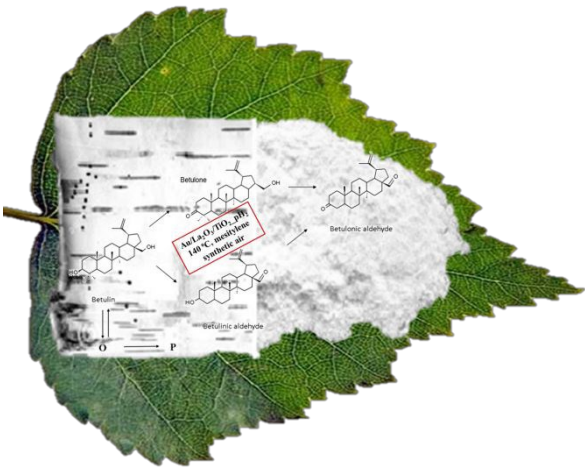
Accepted Manuscripts are published online shortly after acceptance, before technical editing, formatting and proof reading. Using this free service, authors can make their results available to the community, in citable form, before we publish the edited article. We will replace this Accepted Manuscript with the edited and formatted Advance Article as soon as it is available.

You can find more information about Accepted Manuscripts in the [author guidelines](#).

Please note that technical editing may introduce minor changes to the text and/or graphics, which may alter content. The journal's standard [Terms & Conditions](#) and the ethical guidelines, outlined in our [author and reviewer resource centre](#), still apply. In no event shall the Royal Society of Chemistry be held responsible for any errors or omissions in this Accepted Manuscript or any consequences arising from the use of any information it contains.

Betulin can be transformed into its oxo-derivatives by liquid-phase oxidation over gold-based catalysts under mild conditions.

View Article Online
DOI: 10.1039/C9GC00949C



ARTICLE

View Article Online
DOI: 10.1039/C9GC00949C

Oxidation of a wood extractive betulin to biologically active oxo-derivatives using supported gold catalysts

Ekaterina N. Kolobova,^a Ekaterina G. Pakrieva,^a Sonia A.C. Carabineiro,^b Nina Bogdanchikova,^c Andrey N. Kharlanov,^d Sergey O. Kazantsev,^e Jarl Hemming,^f Päivi Mäki-Arvela,^f Alexey N. Pestryakov,^a Dmitry Yu. Murzin^{*f}

Betulin (90-94%) was extracted from birch with a non-polar solvent and recrystallized from 2-propanol. Liquid-phase oxidation of betulin aiming to obtain its biologically active oxo-derivatives (betulone, betulonic and betulinic aldehydes), exhibiting e.g. antitumor, anti-inflammatory, antiparasitic, anticancer and anti-HIV properties, was demonstrated for the first time over gold-based catalysts. Gold was deposited on pristine TiO₂ and the same support modified with ceria and lanthana, followed by pretreatment with H₂ or O₂ atmosphere. The catalysts were characterized by XRD, BET, ICP, TEM, XPS, DRIFT CO, TPD of NH₃ and CO₂ methods. The nature of the support, type of modification and the pretreatment atmosphere through the metal-support interactions significantly influenced the average particle size of gold, its distribution and the electronic state of gold, as well as the acid-base properties and, thereby, the catalytic performance (activity and selectivity) in betulin oxidation. Au/La₂O₃/TiO₂ pretreated in H₂ displayed the highest catalytic activity in betulin oxidation among the studied catalysts with selectivities to betulone, betulonic and betulinic aldehydes of 42, 32 and 27%, respectively, at 69% conversion. Side reactions resulting in oligomerization/polymerization products were occurring on the catalyst surface with the participation of strong acid sites, diminishing the yield of the desired compounds. The latter was improved by adding hydrotalcite with the basic properties to the reaction mixture containing the catalyst. Kinetic modelling through numerical data fitting was performed to quantify the impact of such side reactions and determine the values of rate constants.

Received 00th January 20xx,
Accepted 00th January 20xx

DOI: 10.1039/x0xx00000x

Introduction

Utilisation of natural compounds for chemical transformations to obtain biologically active compounds has become one of the promising and actively developing areas of fine organic synthesis and pharmaceutical chemistry. Triterpenoids are a class of compounds that combine accessibility, i.e., availability in nature and easiness of isolation, with valuable biological activity. Betulin (lup-20 (29) -ene-3, 28-diol, C₃₀H₅₀O₂, CAS: 473-98-3) – a pentacyclic triterpenoid of the lupane series, is found in almost two dozen plants belonging to different genera and families, wherein the main source of betulin is birch bark with the content varying from 10 to 35%. The methods of betulin extraction from birch bark are widely reported in the literature including extraction of the bark outer layer by various solvents, bark alkaline hydrolysis followed by ethanol extraction of betulin, “explosive” autohydrolysis, etc.¹⁻⁶ Betulin and especially its oxo-derivatives (betulone, betulonic and betulonic aldehydes,

betulinic and betulonic acids) have valuable biologically active properties, and are of exceptional interest for the pharmaceutical, cosmetic and food industries.⁶⁻⁹ For example, betulinic acid and its derivatives exhibit anti-cancer, anti-HIV, antiviral, anti-inflammatory, antiseptic, antimicrobial, anti-malarial, anti-leishmaniasis, anthelmintic and fungicidal activity. While betulonic acid has pronounced anti-inflammatory, antimelanomas and antiviral effects. Antiviral and anti-leukemic activity was also reported for betulonic aldehyde, which is, moreover, active against diseases of the liver, the digestive tract and disorders of reproductive function. The 3-oxo derivative of betulin – betulone and its derivatives, exhibiting antitumor, anti-inflammatory, antiparasitic, anti-HIV properties, also demonstrate in vitro cytotoxic activity against different cancer cell lines.¹⁰⁻²² Recent studies indicate a clear demand for betulone as a building block for creating effective anticancer agents with minimal side effects.²⁰⁻²²

Currently, the main method of synthesis of betulin oxo-derivatives is its oxidation. The work of Csuk et al.²³ described formation of betulinic acid via betulinic aldehyde by oxidation of betulin with a mixture comprising TEMPO (2,2,6,6-tetramethylpiperidine-1-oxyl) - NaClO₂ - NaOCl at 35°C with 92% yield. Synthesis of betulinic acid from betulin can be carried out in one stage using butyl acetate with 4-acetamido-TEMPO and Bu₄NBr·H₂O as oxidants in an aqueous solution of NaClO₂ and NaOCl at 50°C, regulating pH with phosphate buffer. Methods of obtaining betulonic acid and betulonic aldehyde by betulin oxidation with chromium oxide (VI), chlorochromate or pyridinium dichromate fixed on a solid silica gel or alumina were also reported. Betulinic acid was synthesized by oxidation of betulonic aldehyde with potassium permanganate.²⁴ A method for selective oxidation of betulin with

^a Research School of Chemistry & Applied Biomedical Sciences, Tomsk Polytechnic University Lenin Avenue 30, 634050 Tomsk, Russia.

^b Laboratory of Catalysis and Materials (LCM), Associate Laboratory LSRE-LCM, Department of Chemical Engineering, Faculty of Engineering, University of Porto Rua Dr Roberto Frias s/n, 4200-465 Porto, Portugal.

^c Centro de Nanociencias y Nanotecnología, UNAM Post box 14, 22860 Ensenada, México.

^d Department of Chemistry, M.V. Lomonosov Moscow State University, Leninskie Gory, 119991 Moscow, Russia.

^e Institute of Strength Physics and Materials Science of Siberian Branch of Russian Academy of Sciences (ISPMS SB RAS) pr. Akademicheskii 2/4, 634055 Tomsk, Russia.

^f Johan Gadolin Process Chemistry Centre, Abo Akademi University FI-20500 Turku, Finland. E-mail: d.murzin@abo.fi; Fax: +358 2 215 4479; Tel: +358 2 215 4985

* Electronic Supplementary Information (ESI). See DOI: 10.1039/x0xx00000x



pyridinium dichromate (PDC), pyridinium chlorochromate (PCC) or $K_2Cr_2O_7$ - 9M H_2SO_4 in the presence of tetrabutylammonium bromide (TBAB) to betulinic aldehyde, or its mixture with betulonic aldehyde and ketol was developed by Komissarov et al.²⁵ The yield of oxidation products did not exceed 75%. The method of obtaining betulonic acid by oxidation of betulin, in the first step with the Jones reagent in acetone, should also be mentioned.^{26,27} Alternatives include application of the pyridine dichromate complex and acetic anhydride in dimethylformamide,²⁸ and chromium (VI) oxide in acetic acid, followed by reduction to betulinic acid.²⁹ Two-stage methods for synthesis of betulinic acid have significant shortcomings. Low solubility of betulin in acetic acid, acetone and methylene chloride and of betulonic acid and its salts in alcohols, tetrahydrofuran and water, imposes several limitations, preventing oxidation and reduction and, thus, resulting in poor yields and purity. In the majority of the proposed oxidation methods, highly toxic Cr (VI) is used. Moreover, separation of the products containing toxic Cr (III) ions is very laborious and time consuming.

In addition to chemical modifications, attempts to transform betulin using microorganisms were carried out, mainly for synthesis of betulone.^{10,30-33} However, such betulin biotransformation processes using conditionally pathogenic yeasts, fungi, etc. have significant drawbacks, requiring complex nutrient media, long duration, low concentration levels of products as the biocatalyst might not tolerate higher concentrations.

Recently,^{34,35} some of the authors of this work demonstrated for the first time the possibility to selectively oxidize betulin to betulinic aldehyde using Ru/C as a catalyst mixed with the basic hydrotalcite and SiO_2 as a dehydrating agent at 108°C in toluene, with air as an oxidant. Under these conditions, the conversion of betulin after 24 hours was 41% with 67% selectivity to betulinic aldehyde, whereas without the addition of SiO_2 , conversion and selectivity were 20% and 66%, respectively. A higher conversion was achieved when the reaction was carried out in an acidic medium, giving, however, allobetulin as the main product. It was found that the presence of a basic agent and elimination of water are crucial for selective oxidation of betulin to betulinic aldehyde on Ru catalysts. Selective oxidation of betulin to betulone was also reported using silver supported on unmodified titania and modified with ceria under mild conditions, e.g. atmospheric pressure, relatively low temperature (140°C), synthetic air as an oxidant, solvent – mesitylene. Conversion of betulin over Ag/CeO₂/TiO₂ catalyst reached 27% after 6 hours, which was substantially larger than 11% obtained for Ag/TiO₂. In all cases the main product was betulone with selectivity exceeding 60%.

Based on the analysis of published studies on betulin oxidation, it is obvious that currently there are no economically and ecologically acceptable methods for producing oxo-betulin derivatives. Such methods based on heterogeneous catalysis should replace existing stoichiometric processes which lead to formation of large amounts of toxic waste, being able to provide preferably a quantitative yield of the desired product. In the present work, the possibility of heterogeneous catalytic oxidation of betulin with synthetic air, using catalysts based on gold nanoparticles supported on unmodified and modified titania, will be demonstrated for the first time. Some of these catalysts have been synthesized before and used for oxidation

of octanol³⁷ which has, however, chemical and physical properties different from those for betulin. No reports on betulin oxidation over gold catalysts are available in the literature, thus it was interesting to explore possibility of their utilization for a much more complex case than oxidation of octanol.

The aim of the present study is thus to evaluate applicability of gold-based catalysts in the liquid phase selective oxidation of betulin, to elucidate the influence of the support and nature of the additives, the impact of redox pretreatment on catalytic properties.

Moreover, a comparative analysis of the catalytic properties of ruthenium, silver and gold catalysts in betulin oxidation was performed showing that the latter ones are more active and stable.

Results and discussion

XRD was used to study the phase composition of the investigated catalysts (ESI Fig. S1[†]). The XRD patterns showed absence of the reflections characteristic for gold and modifiers, indicating small sizes of gold and metal oxides particles (lower than the sensitivity XRD threshold of 3–4 nm) or their X-ray amorphous structure.

Table 1 shows the specific surface area of supports and catalysts (S_{BET}), Au content and gold particle size data. The surface area of the pristine TiO₂ was diminished by 13% after modification (48 m²/g) with both modifiers. Further gold deposition did not significantly change the specific surface area of the supports, except Au/La₂O₃/TiO₂, for which there was a noticeable decrease by 10% (Table 1). ICP analysis showed that Au contents were close to the nominal ones.

The average size of gold nanoparticles is lower than 3 nm for most of the studied materials, except Au/TiO₂-pO₂ (Table 1). The largest size of gold nanoparticles and the broadest distribution were observed in the case of gold supported on unmodified titania (ESI Fig. S2[†]). On the contrary, for La-modified materials, the size of Au particles and the range of their distribution are the smallest. These values for Ce-modified materials were in between other catalysts. In addition to the support nature, the pretreatment atmosphere (H_2 or O_2) also affects the uniformity of particles and their relative size. At the same time, the impact of pretreatment depends also on the support. For unmodified and lanthana-modified materials, smaller particles were obtained after pretreatment in H_2 (300°C), and for ceria-modified after O_2 (300°C). These effects can be attributed to the specificity of gold interactions with different supports during catalyst preparation, as previously confirmed,³⁶ and to the different nature of the gold precursor decomposition under reducing and oxidizing pretreatment, previously revealed by TPR.³⁷ It should also be taken into account that a certain fraction of gold is in the form of highly dispersed oxidized gold species, which are quite difficult to be detected by electron microscopy because of the lower contrast of oxidized species compared to the reduced ones. The presence of such oxidized species was previously validated by TPR.³⁷ Moreover, gold in the ionic state (Au^+ or Au^{3+}) not detected by TEM, could still be present, according to DRIFT CO



and XPS (Fig. 1 and Table 2). The amount of these gold species (ionic and oxidized gold species) depends on the support and pretreatment.

Table 1 Textural properties of supports and catalysts, analytical contents of Au, dispersion and average particle size of gold

Sample	S_{BET} , m ² /g	Au conten t wt.% by ICP*	Au average nanoparticl e size, nm	Dispersion , %
TiO ₂	55	-	-	
La ₂ O ₃ /TiO ₂	48	-	-	
CeO ₂ /TiO ₂	48	-	-	
Hydrotalcite	43	-	-	
Au/TiO ₂ _pH ₂	50	4.0	2.9	34
Au/TiO ₂ _pO ₂	50	4.0	3.3	30
Au/CeO ₂ /TiO ₂ _pH	46	4.1	2.8	36
² Au/CeO ₂ /TiO ₂ _pO ₂	46	4.1	2.4	42
Au/La ₂ O ₃ /TiO ₂ _pH	43	3.3	2.6	38
² Au/La ₂ O ₃ /TiO ₂ _pO	43	3.3	2.7	37

*Data from.³⁷

Table 2 shows the relative atomic concentrations of various electronic states of gold, calculated according to XPS. As can be seen, the relative values of different gold states depend strongly on the support and pretreatment conditions. On the surface of all studied catalysts, most of the gold (68 – 89%) is in a metallic state with BE(Au4f_{7/2}) in the range of 84.2 – 84.3 eV, but also a part of gold (11 – 20%) is in the form of single charged ions (Au⁺) with BE(Au4f_{7/2}) in the range of 85.2 – 85.5 eV. In the case of unmodified and Ce-modified samples pretreated in H₂, another state related to three-charged gold (Au³⁺) with BE(Au4f_{7/2}) equal to 86.5 and 86.3 eV appears in the XPS spectrum (11 and 12%, respectively). These data confirm that the formation of the active surface on different supports, under the action of various pretreatments, occurs differently, and are in good agreement with TEM (Table 1).

Table 2 Electron states of Au calculated according to XPS for the studied catalysts

Sample	Au ^(0, +1 or +3) content in the samples, %		
	Au ⁰	Au ⁺	Au ³⁺
Au/TiO ₂ _pH ₂ *	74	15	11
Au/TiO ₂ _pO ₂ *	89	11	0
Au/CeO ₂ /TiO ₂ _pH ₂	68	20	12

Au/CeO ₂ /TiO ₂ _pO ₂	83	11	6
Au/La ₂ O ₃ /TiO ₂ _pH	81	19	0
² Au/La ₂ O ₃ /TiO ₂ _pO	83	17	0

*Data from.³⁷

For a more detailed study of the electronic state of gold in the investigated catalysts, and also as for the evaluation of the strength and stability of the adsorption centers, DRIFT spectroscopy of adsorbed CO was applied. CO adsorption was carried out at different pressures: 5, 20, and 50 Torr, making it possible to evaluate the strength of the centers. Pure supports did not exhibit bands of adsorbed CO in this region of the spectrum under the studied conditions. From Fig. 1, it can be concluded that for all catalysts, regardless of the pretreatment, one absorption band with the maximum in the range of 2100 – 2120 cm⁻¹, attributed to the surface carbonyls of gold atoms Au⁰-CO,³⁸ was observed. The intensity of this band increased with increasing CO pressure. Differences in the signal position are caused by CO adsorption on the metal clusters of different size, bands with low-frequency associated with larger nanoparticles. CO starts to adsorb on larger gold clusters as the pressure increases. Moreover, carbon monoxide is very weakly adsorbed on metallic gold because of some features of σ-π binding in M⁰-CO for Au, in comparison to other noble metals (Pt, Pd, Ru, Rh, Cu).³⁹ Only highly dispersed gold clusters or atoms can be sites for CO adsorption. This explains different intensities of the absorption bands corresponding to Au⁰-CO at CO pressure of 50 Torr. Subsequently, it can be assumed that there are larger particles in Au/TiO₂_pH₂, Au/CeO₂/TiO₂_pH₂, Au/CeO₂/TiO₂_pO₂, and especially Au/La₂O₃/TiO₂_pO₂ catalysts, which were not taken into account when analyzing TEM images because of their relatively low abundance. In our previous study,⁴⁰ there was a similar discrepancy between the average particle size obtained by TEM and SR-XRD. The average particle size of gold obtained from SR-XRD was in good agreement with the catalytic results, and for some catalysts it was larger than the values determined by TEM. Another absorption band with the maximum in the range of 2140 – 2185 cm⁻¹, related to the complexes of ions Au⁺-CO^{41,42} was observed in almost all cases, except Au/TiO₂_pH₂. However, the intensity of this absorption band, as well as its change with pressure variation, are different. This absorption band is less intense than the attributed to Au⁰-CO, and also strongly depends on CO pressure. The intensity increases with the pressure increase. It is interesting to note that, for Au/La₂O₃/TiO₂_pO₂ (Fig. 1f), reduction of Au⁺ sites is observed in the CO atmosphere, which indicates their very low stability. Absence of this absorption band for Au/TiO₂_pH₂ can be due to the presence of only weak Au⁺ sites, and even a CO pressure of 50 Torr is not enough for their identification by DRIFT CO, while according to XPS (Table 2), Au⁺ is 15% of the total amount of gold. It should also be noted that the XPS method determines the ionic states of gold in the near-surface layer, some of which may not be accessible for adsorbed molecules. At the same time, the method of DRIFT adsorbed CO



allows identification of the active sites on the surface available for the reactions.

TPD of NH_3 was used to determine acidity of supports and respective gold catalysts, namely the concentration and strength of acid sites (Table 3 and ESI Fig. S†). Physical adsorption can take place in the case of ammonia TPD, being, however, typical for low temperatures. Therefore, to avoid contribution of physical adsorption, the analysis started from 100 °C.

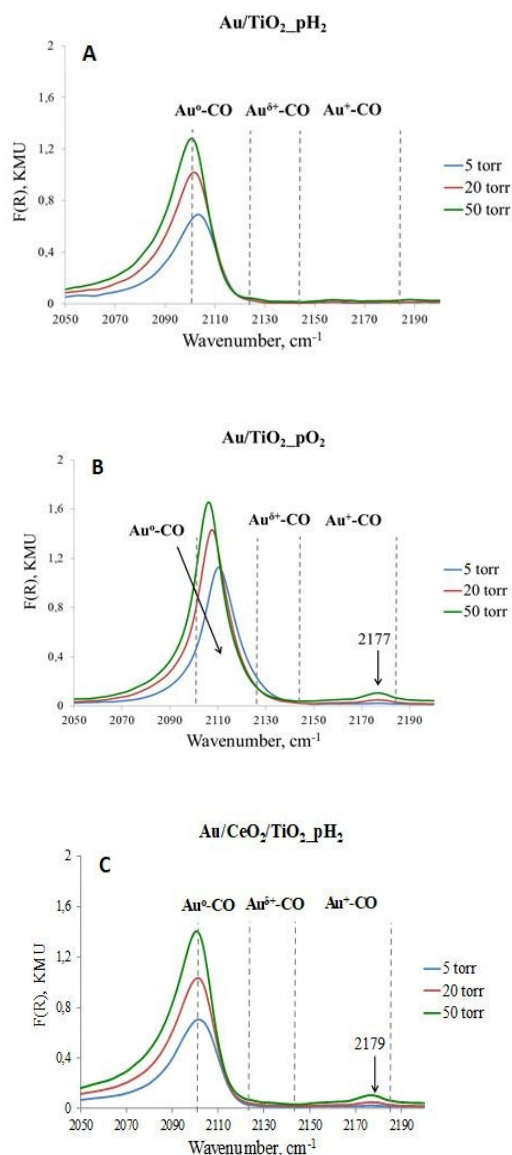


Fig. 1 DRIFT spectra of CO adsorbed on catalysts pretreated at 300°C for 1 h in H_2 or O_2 atmospheres. The spectra of adsorbed CO were recorded at different CO pressures — 5, 20, 50 Torr.

Three types of acid sites are detected for the initial supports, but their concentration and strength are different (Table 3). The pristine titania showed the highest acidity among the used supports with the majority of acidic sites being of weak strength, while the concentration of the medium and strong acidic sites is 2.6 and 6.9 folds lower than the previous one. Therewith, they are all Brønsted acid sites (acidic OH groups).⁴³⁻⁴⁵ However, it is possible that the strong acid sites are of aprotic nature and are Lewis acid sites (e.g. tetrahedral coordinated Ti^{4+}).⁴⁶



Modification of titania with ceria and lanthana led to a decrease in the concentration of weak and medium acid sites. This is most likely a consequence of surface dehydration after calcination at 550°C during preparation. Alongside with that, the amount of strong acid sites increased for Ce-modified, but decreased for La-modified titania. In the case of ceria-modified TiO_2 , this can be explained by the appearance of new Lewis sites, due to the presence of $\text{Ce}^{4+}/\text{Ce}^{3+}$, which existence was indirectly confirmed by TPR.³⁷ For lanthana-modified material, no hydrogen consumption was observed in TPR profiles. Thus, it can be assumed that lanthana blocked the acid sites on the pristine titania surface leading to a decrease in acidity. After gold deposition, in all cases, there was a redistribution of acid sites. Regardless of pretreatment for unmodified and Ce-modified materials, an increase in the concentration of weak acid sites and a significant decrease of strong acid sites were observed. The amount of medium sites in the case of $\text{Au}/\text{CeO}_2/\text{TiO}_2$ was increased, while for Au/TiO_2 it remained almost unchanged. The distribution of acid sites is noticeably different for the La-modified catalyst, compared with the other materials. This is most clearly seen for strong acid sites, which concentration significantly increased. Moreover, there was a decrease of weak acid sites in comparison with unmodified and Ce-modified materials. Such changes in acidity after metal deposition may originate from several reasons. One of the options can be associated with a change in the support properties during catalyst preparation resulting the mutual influence of the support and the metal precursor, as previously discussed.^{36,47-49} Another possibility is blocking the acid sites, previously existing on the surface by newly formed metal nanoparticles. It should be noted that, in the case of La-modified catalyst, a part of the strong acid sites ($90 \cdot 10^{-4} \text{ mol/m}^2$) may be associated with the Lewis acid sites, namely Au^+ . This is confirmed by comparing XPS (Table 2), DRIFT CO (Fig. 1) and NH_3 -TPD (Table 3) data. Considering that lanthana is a non-reducible oxide, it can be suggested that another part of the strong acid sites is associated with Brønsted acidity and belongs to the support or the modifier.

Table 3 Acidic properties of supports and catalysts.

Sample	Concentration of acid sites, $\text{mol} \cdot 10^{-4} / \text{m}^2$			
	weak	medium	strong	total
TiO_2	378	144	55	577
$\text{CeO}_2/\text{TiO}_2$	304	90	115	509
$\text{La}_2\text{O}_3/\text{TiO}_2$	302	90	8	400
$\text{Au}/\text{TiO}_2_{\text{pH}_2}$	528	162	16	706
$\text{Au}/\text{TiO}_2_{\text{pO}_2}$	520	132	18	670
$\text{Au}/\text{CeO}_2/\text{TiO}_2_{\text{pH}_2}$	496	356	80	932
$\text{Au}/\text{CeO}_2/\text{TiO}_2_{\text{pO}_2}$	421	187	69	677
$\text{Au}/\text{La}_2\text{O}_3/\text{TiO}_2_{\text{pH}_2}$	146	135	239	713
$\text{Au}/\text{La}_2\text{O}_3/\text{TiO}_2_{\text{pO}_2}$	276	286	170	732

In order to assess the basic properties of the studied materials TPD of CO_2 was used. Based on the literature,⁵⁰⁻⁵³ depending on the

temperature range in which CO_2 desorption occurs, the basic sites are divided into three types: weak, medium and strong, reflecting their nature. The weak basic sites (25 - 200°C) are usually attributed to surface hydroxyl groups, medium ones (200 - 400°C) to metal oxide pairs, and strong sites (400 - 600°C) to low-coordinated oxygen anions. All types of basic sites mentioned above were observed for the supports studied in this work (Table 4 and ESI Fig. S4[†]). Pristine titania exhibited the average total basicity among the studied supports, with the dominance of basic sites of medium strength and almost absent strong sites. A similar distribution of the basic sites was also observed for Ce-modified titania, while the amount of these sites was lower. After modification of titania by lanthana, there was an increase in the concentration of weak and strong basic sites, while the amount of medium sites remained almost unchanged. Table 4 also presents the results for hydrotalcite, basicity of which is 2-3 folds higher than of the used supports. The gold deposition on the support surface led to a redistribution of the basic sites similar to the acidic ones (Table 3). For almost all studied catalysts, there was an increase in the amount of basic sites while, in all cases, the strong basic sites increased. The reasons for the changes in basicity after gold deposition are apparently the same as for acidity in a sense that they originate from exposure of the support to the metal precursor during preparation, mutual influence of the support and the precursor, and base site blocking.

In addition, as shown in,^{54,55} CO_2 is also capable of being adsorbed on small gold nanoparticles, with abstraction of oxygen by Au^0 , giving CO and $\text{Au}_2^+\text{O}^{2-}$ species, which cannot be considered as the basic sites. When comparing CO_2 -TPD (Table 4) and TEM (Table 1), it can be concluded that the highest increase in the amount of basic sites was observed for samples with the smallest particle sizes. Subsequently, a part of the strong basic sites can be associated with CO_2 adsorption on small gold nanoparticles.

Table 4 Basic properties of supports and catalysts

Sample	Concentration of basic sites, $\text{mol} \cdot 10^{-4} / \text{m}^2$			
	weak	medium	strong	total
TiO_2	53	93	9	155
$\text{CeO}_2/\text{TiO}_2$	56	83	6	145
$\text{La}_2\text{O}_3/\text{TiO}_2$	117	96	35	248
Hydrotalcite	284	230	37	555
$\text{Au}/\text{TiO}_2_{\text{pH}_2}$	30	85	34	149
$\text{Au}/\text{TiO}_2_{\text{pO}_2}$	68	58	42	168
$\text{Au}/\text{CeO}_2/\text{TiO}_2_{\text{pH}_2}$	130	137	67	334
$\text{Au}/\text{CeO}_2/\text{TiO}_2_{\text{pO}_2}$	43	67	52	162
$\text{Au}/\text{La}_2\text{O}_3/\text{TiO}_2_{\text{pH}_2}$	88	107	177	372
$\text{Au}/\text{La}_2\text{O}_3/\text{TiO}_2_{\text{pO}_2}$	51	88	74	213

Catalytic behavior of Au supported catalysts in the betulin liquid phase oxidation (Figure 2) was studied at 140°C and a synthetic air pressure of 1 bar in mesitylene. To assess the influence of the support nature and pretreatment atmosphere, gold was deposited



on pristine titania and TiO_2 modified with ceria and lanthana. The obtained materials were pretreated in H_2 or O_2 .

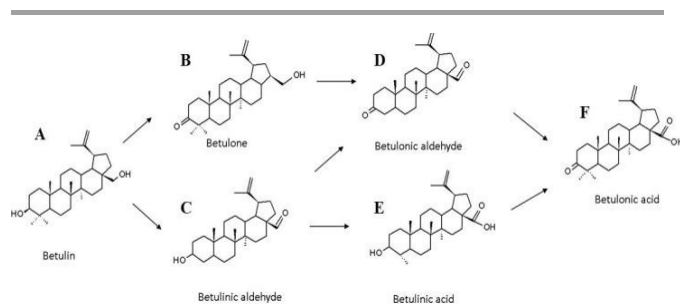


Fig. 2 Reaction scheme for betulin oxidation.

It was found that both the nature of the support and the pretreatment atmosphere have a significant influence on the catalytic behavior of the studied catalysts (Table 5). Among the studied gold containing materials, Au/TiO_2 pretreated in H_2 (Table 5, entry 1) had the lowest activity. Betulin (A) conversion was 25%, with selectivity to betulone (B) and betulinic aldehyde (C) of 40 and 53%, at this conversion level, respectively. Herewith, the total yield of products was only 15%, which is 1.7 fold lower than the observed conversion (Table 5 - entry 1, Fig. 3a,d). This difference is due to incomplete mass balance (the sum of the masses of the reactant and products visible in GC, GCLPA). This is most likely caused by strong adsorption of reactants or products on the catalyst surface. The mass balance closure was different for the various catalysts, being

determined by the catalyst properties. In this particular case, the GCLPA was 90%. Betulin conversion and selectivity for the same material (Au/TiO_2), but pretreated in O_2 , were almost the same (Table 5, entry 2). However, due to a better GCLPA - 96%, the total yield of products for this catalyst turned out to be 1.7 fold higher than for the one pretreated in H_2 .

In contrast to the unmodified material, betulin conversion for Ce-modified catalyst was higher after the pretreatment in H_2 (betulin conversion - 45%, Table 5, entry 3). However, the mass balance closure in this case was the worst - 77%, ultimately giving only 22% total yield of the main products. For the same catalyst, but pretreated in oxygen, a lower conversion - 33%, was achieved (Table 5, entry 4). The best 95% GCLPA was, however, reached for this case, with the total yield of products being 1.2 fold higher than after pretreatment in H_2 . The pretreatment atmosphere even affected selectivity for the primary products, such as betulone (B) and betulinic aldehyde (C), which should be less sensitive to conversion levels. For $\text{Au/CeO}_2/\text{TiO}_2_{\text{pO}_2}$ in particular, the main product was betulinic aldehyde (C), while for $\text{Au/CeO}_2/\text{TiO}_2_{\text{pH}_2}$ betulone (B) was mainly obtained.

$\text{Au/La}_2\text{O}_3/\text{TiO}_2$ pretreated in hydrogen had the highest activity among the studied catalysts. Betulin conversion was 69% and the main products were betulone (B), betulonic (D) and betulinic (C) aldehydes, with selectivities of 42, 32 and 27%, respectively (Table 5 - entry 5, Figure 3b,d). It should be noted that due to GCLPA of 80%, the total yield of the main products turned out to be 1.4 fold lower than the observed conversion, being 48%. Betulin conversion for the same material ($\text{Au/La}_2\text{O}_3/\text{TiO}_2$), but pretreated in O_2 was 2.8 fold lower than after treatment in H_2 (Table 5, entry 6).

Table 5 Catalytic behaviour of Au, Ru and Ag supported catalysts in betulin oxidation

Entry	Catalyst	X (%)	GCLPA (%)	Selectivity, %						$\Sigma Y_{\text{product}}$ (%)
				S_B	S_D	S_F	S_C	S_E	$S_{\text{allobetulin}}$	
1	TiO_2	13	93	65	3	5	15	2	0	6
2	$\text{CeO}_2/\text{TiO}_2$	17	91	69	9	0	0	22	0	8
3	$\text{La}_2\text{O}_3/\text{TiO}_2$	4	97	53	47	0	0	0	0	3
4	$\text{Au/TiO}_2_{\text{pH}_2}$	25	90	40	6	tr.	53	1	0	15
5	$\text{Au/TiO}_2_{\text{pO}_2}$	27	96	38	10	1	51	tr.	0	25
6	$\text{Au/CeO}_2/\text{TiO}_2_{\text{pH}_2}$	45	77	48	11	tr.	40	1	0	22
7	$\text{Au/CeO}_2/\text{TiO}_2_{\text{pO}_2}$	33	95	34	11	1	54	0	0	27
8	$\text{Au/La}_2\text{O}_3/\text{TiO}_2_{\text{pH}_2}$	69	80	42	32	tr.	27	0	0	48
9	$\text{Au/La}_2\text{O}_3/\text{TiO}_2_{\text{pO}_2}$	25	97	44	7	1	48	0	0	22
10	$\text{Au/La}_2\text{O}_3/\text{TiO}_2_{\text{pH}_2}^a$	70	85	54	25	0	21	0	0	55
11	$\text{Au/La}_2\text{O}_3/\text{TiO}_2_{\text{pH}_2}^b$	71	87	52	27	0	21	0	0	58
12	$\text{Au/La}_2\text{O}_3/\text{TiO}_2_{\text{pH}_2}^c$	48	87	57	24	0	19	0	0	35
13	$\text{Au/La}_2\text{O}_3/\text{TiO}_2_{\text{pH}_2}^d$	58	88	64	19	tr.	17	tr.	0	46
14	Ru/C , Degussa ^d	54*	-	0	2	1	16	2	72	-
15	Ru/C , Degussa ^{d,e}	16*	-	0	9	5	77	0	2	-
16	Ru/C , Degussa ^f	12*	-	0	13	49	37	0	1	-
17	Ru/C , Degussa ^{d,g}	41**	-	0	8	4	67	4	4	-
18	Ag/TiO_2	11	-	59	8	3	21	3	0	-
19	$\text{Ag/CeO}_2/\text{TiO}_2$	27	-	60	4	1	6	7	0	-



Conditions: 140°C, synthetic air (50 ml/min) as oxidant, solvent - mesitylene, entries 1-12, 18 and 19; X – conversion of betulin after 6 h (%); GCLPA - the sum of reactant and product masses in GC analysis (%); S_B – selectivity to betulone (%); S_D – selectivity to betulonic aldehyde (%); S_F – selectivity to betulonic acid (%); S_C – selectivity to betulonic aldehyde (%); S_E – selectivity to betulonic acid (%); $S_{allobetulin}$ – selectivity to allobetulin (%); $\Sigma Y_{product}$ – total product yield after 6 h (%); tr. – traces; ^awith 0.2 g of hydrotalcite; ^bwith 0.2 g of hydrotalcite and 0.2 g SiO₂; ^csecond run; ^dconditions: 108°C, synthetic air (50 ml/min) as oxidant, solvent – toluene, entries 13 - 17; ^ewith 0.5 g of hydrotalcite; ^fconditions are the same as for entries 1-12; ^gwith 0.5 g of hydrotalcite + 0.5 g SiO₂; *conversion of betulin after 5 h (%); **conversion of betulin after 24 h (%); data of 14 - 17 entries from³⁴; data of 18 and 19 entries from³⁵.

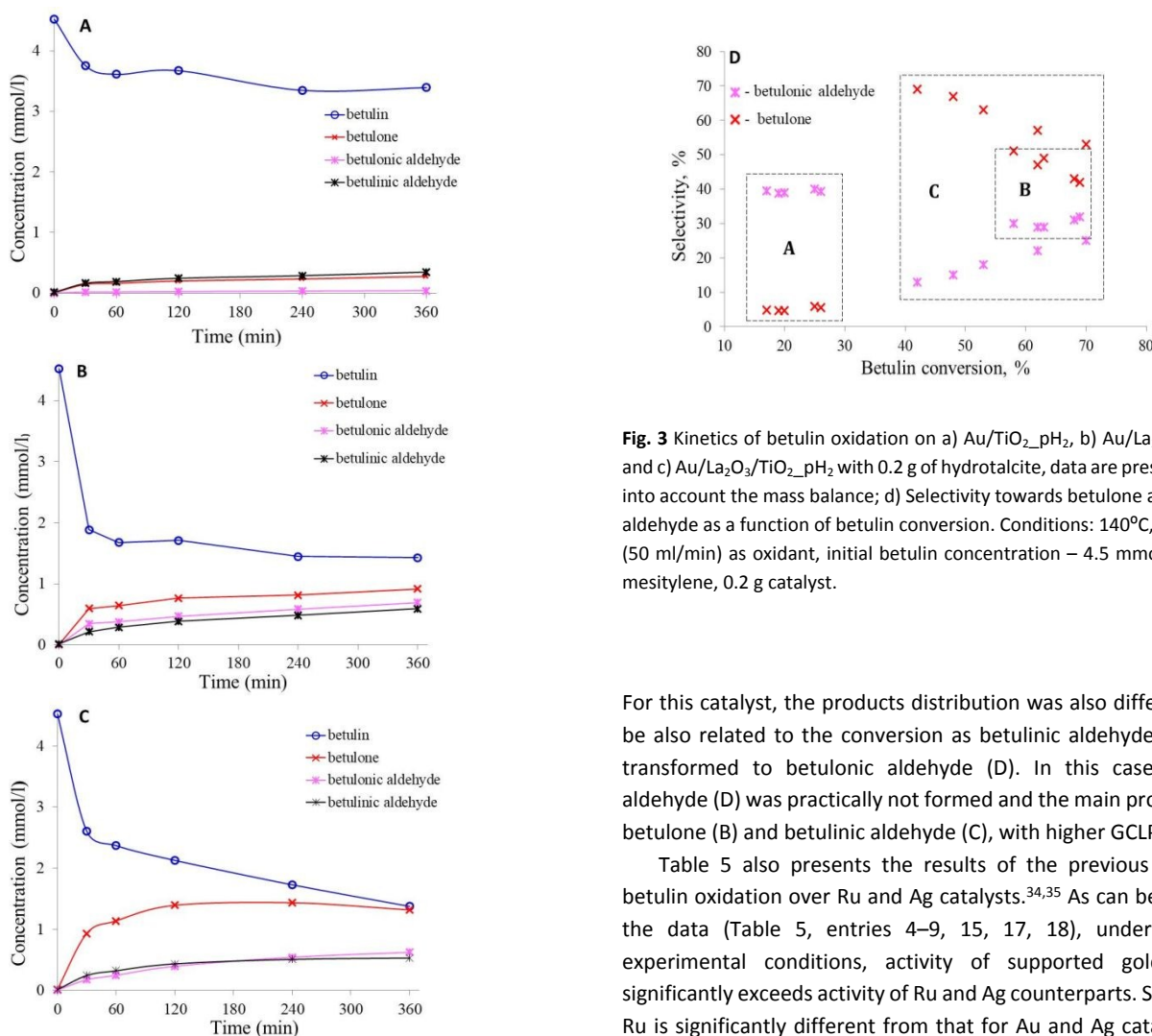


Fig. 3 Kinetics of betulin oxidation on a) Au/TiO₂-pH₂, b) Au/La₂O₃/TiO₂-pH₂ and c) Au/La₂O₃/TiO₂-pH₂ with 0.2 g of hydrotalcite, data are presented taking into account the mass balance; d) Selectivity towards betulone and betulonic aldehyde as a function of betulone conversion. Conditions: 140°C, synthetic air (50 ml/min) as oxidant, initial betulin concentration – 4.5 mmol/l, solvent - mesitylene, 0.2 g catalyst.

For this catalyst, the products distribution was also different. It can be also related to the conversion as betulonic aldehyde (C) can be transformed to betulonic aldehyde (D). In this case, betulonic aldehyde (D) was practically not formed and the main products were betulone (B) and betulonic aldehyde (C), with higher GCLPA (97%).

Table 5 also presents the results of the previous studies on betulin oxidation over Ru and Ag catalysts.^{34,35} As can be seen from the data (Table 5, entries 4–9, 15, 17, 18), under the same experimental conditions, activity of supported gold catalysts significantly exceeds activity of Ru and Ag counterparts. Selectivity of Ru is significantly different from that for Au and Ag catalysts. Over the majority of Au(Ag)/(modifier)/TiO₂ catalysts the main reaction products were betulone (B) and betulonic aldehyde (C), while betulonic acid (F) and betulonic aldehyde (C) were obtained for Ru/C. It is also worth noting that allobetulin was not observed in the reaction products for Au(Ag)/(modifier)/TiO₂ in comparison with Ru. Moreover in the previous work the mass balance closure was not explicitly accounted for, making a direct comparison of the yields not straightforward.

In the work,³⁴ it was also shown that the catalytic behavior (activity and selectivity) of Ru catalysts depends strongly on the reaction conditions. In toluene as a solvent at 108 °C, betulin



conversion over Ru/C (entry 14) was 54% after 5 hours with allobetulin (77%), a structural isomer of betulin, as the main product. To evaluate how the reaction conditions affect the catalytic behavior of gold materials, a similar experiment was carried out using Au/La₂O₃/TiO₂_pH₂ in toluene at 108 °C (entry 13). Compared with entry 8, betulin conversion decreased 1.2 fold, however, the main reaction products were still betulone (B), betulonic (D) and betulinic (C) aldehydes. It is worth noting that in this case, the mass balance closure was higher (88%) compared with entry 8 (80%), therefore, the difference in $\sum Y_{\text{product}}$ between 8 and 13 entries was only 2%.

Selectivity to a more desired product (betulinic aldehyde as opposed to allobetulin) was increased³⁴ by adding basic hydrotalcite to the reaction mixture, even if there was a negative influence on activity decreasing betulin conversion from 54% to 16%, Table 5, entry 15. The betulin conversion reached 41% with selectivity to betulinic aldehyde 67% (Table 5, entry 17) with increasing reaction time up to 24 hours, adding hydrotalcite and silica as a dehydrating agent. In the present work, a similar experiment was carried out, and hydrotalcite was added to the reaction mixture containing Au/La₂O₃/TiO₂_pH₂ (Table 5, entry 10, Fig. 3c,d). However, there were no significant changes in betulin conversion or in the product distribution. Betulin conversion increased by only 1% after adding hydrotalcite. Despite a slight increase in betulin conversion, TOF increased 1.4 fold and was 0.010 s⁻¹, compared to the experiment without hydrotalcite, for which it was 0.007 s⁻¹. Moreover, due to the better GCLPA – 85%, the total yield of the main products increased to 55% compared with entry 5, being 48% (Table 5). Addition of silica to the reaction mixture, along with Au/La₂O₃/TiO₂_pH₂ and hydrotalcite, additionally increased betulin conversion by 1% and products yield by 3%, as well as GCPLA to 87% (Table 5, entry 11). Thus, it can be assumed that addition of hydrotalcite, giving apparently local changes in concentrations of proton and hydroxyls in the vicinity of the catalyst surface, can thereby affect the properties of the catalyst surface. In turn, silica prevents the inhibitory action of water. However, in the case of betulin oxidation over gold catalysts, inhibition by water is much less pronounced than for Ru catalysts.³⁴ In general, gold materials were less sensitive to changes in the reaction conditions than ruthenium ones. When Au/La₂O₃/TiO₂_pH₂ was recycled (Table 5, entry 12), a 30% drop in activity compared to entry 8 was observed, indicating some catalyst deactivation. However, the gold catalyst was still more stable than ruthenium, for which the activity decreased by 44% in the second run (from 41% to 23%).³⁴ As mentioned above in Introduction betulone is equally important as betulinic aldehyde or betulinic acid. Selectivity to betulone can be increased by adding to the reaction mixture besides the catalyst also hydrotalcite and silica or by replacing the solvent and lowering the reaction temperature.

When comparing GCLPA for the same catalyst, but pretreated in different atmospheres (e.g. Au/La₂O₃/TiO₂_pH₂ and Au/La₂O₃/TiO₂_pO₂, Table 5, entries 4 – 8) with acid-base properties (Table 3 and 4), it can be assumed that GCLPA is determined by the acidity of the materials, namely the concentration of medium and

strong acid sites. The lower is this concentration, the higher the mass balance closure (Figure 4), which can be explained by side reactions, promoted on stronger sites leading to lower GCLPA. This is also confirmed by comparing the catalytic and ammonia TPD data for the supports applied in this work (Table 3, Table 5 – entries 1-3). For Ce-modified TiO₂, the concentration of medium and strong acid sites was the highest among supports, and the GCPLA was the lowest. For La-modified TiO₂, the opposite situation was observed. From this point of view, hydrotalcite indirectly affected the catalyst properties, in particular the strong acid sites, preventing the side reactions and increasing the product yield.

Along with the acidity of the materials, their basicity also plays an important role (Table 4). Betulin conversion was higher for catalysts with more pronounced basic properties. Herewith, H₂-pretreated materials were more basic, but at the same time, they also demonstrated higher acidity. The exception was Au/TiO₂, for which conversion or the product distribution was almost independent of the pretreatment atmosphere. This can be explained that the acid-base properties of this material vary only slightly upon different pretreatment.

It should be noted that while a certain correlation between the acid-base properties and catalytic performance was seen, the role of gold in betulin oxidation is decisive. Moreover, correlations between TPD of ammonia and CO₂ made in the gas-phase with catalytic properties should be taken with caution when the catalysts are employed in the liquid-phase processes. Nevertheless, TPD methods provide general information on the nature of solid surfaces and the types of sites and are often applied for characterizing the acid-base properties of solid catalysts even for the liquid phase reactions.

In order to find out the reason for a decrease in GCPLA, namely, what was adsorbed on the catalyst surface, size exclusion chromatography (SEC) was used.

After carrying out the extraction and SEC analysis, it was found that polymers and oligomers with a molecular weight of 5000 and 1000 Da, respectively, were formed on the catalyst surface (ESI Fig. S5⁺). The weight of oligomers/polymers on the catalyst was not quantified, being, however, related to the mass imbalance between the theoretical GCLPA (100%) and the corresponding values of GCLPA reported in Table 5.

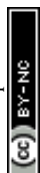
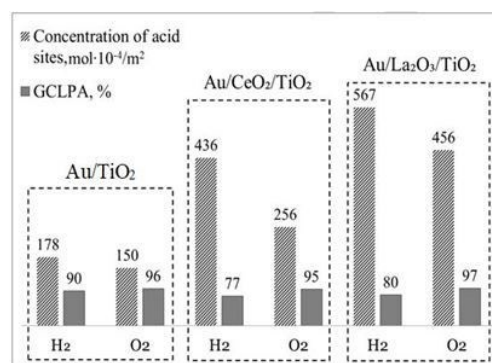


Fig. 4 Dependence of GCLPA on concentration of medium and strong acid sites.

Thus, it can be concluded that a decrease in GCPLA is associated with side reactions of betulin or its derivatives oligomerization/polymerization on the catalyst surface, with the participation of strong acid sites. Formation of oligomers/polymers on the catalyst surface is also likely to cause partial deactivation of the recycled catalyst (Table 5, entry 12). Despite washing the catalyst after the first run in hot acetone, a part of the oligomers/polymers could remain on the surface thereby blocking partially active sites. This is also confirmed by an increase in GCPLA after the second run (Table 5, entry 12).

In order to quantify the kinetic significance of various steps comprising the reaction network and a contribution of side reactions leading to oligomers/polymers, kinetic modelling was performed for betulin oxidation in the presence of Au/La₂O₃/TiO₂-pH₂ and hydrotalcite (Fig. 3c). The reaction scheme given in Fig. 2 was somewhat modified (Fig. 5) to incorporate formation of oligomers (O) and finally polymers (P) and account for a clear lack of mass balance closure in Fig. 3c. The reaction scheme was simplified as the concentration of acids was negligible for Au/La₂O₃/TiO₂-pH₂. In general, oligomers can originate not only from the reactant as in Fig. 5 but also from the products, as mentioned above. However, a lack of mass balance closure in some cases was seen already at the beginning of experiments justifying that the main contribution for formation of oligomers comes from the reactants. To keep a more general character of the model, formation of oligomers was considered to be reversible, while generation of polymers as terminal species was supposed to be irreversible.

The equations for the reaction rates presented in Fig. 5 can be easily written:

$$r_1 = \frac{k_1 K_A C_A}{(1 + \sum K_i C_i)}, r_2 = \frac{k_2 K_A C_A}{(1 + \sum K_i C_i)}, r_3 = \frac{k_3 K_C C_C}{(1 + \sum K_i C_i)}, r_4 = \frac{k_4 K_B C_B}{(1 + \sum K_i C_i)},$$

$$r_5 = \frac{k_5 K_A C_A - k_{-5} K_O C_O}{(1 + \sum K_i C_i)}, r_6 = \frac{k_6 K_O C_O}{(1 + \sum K_i C_i)} \quad (1)$$

These equations correspond to adsorption of all organic compounds and subsequent oxidation with noncompetitively adsorbed oxygen. Dependence of the oxygen concentration is thus implicitly incorporated in the rate constants k_i .

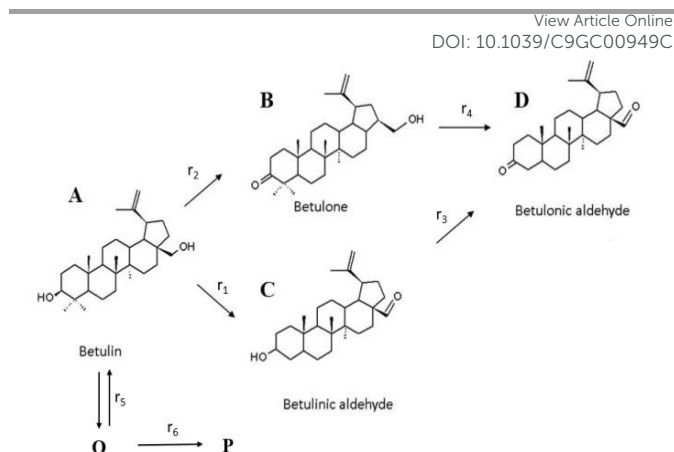


Fig. 5 Modified reaction scheme for betulin oxidation, which includes formation of oligomers (O) and polymers (P).

In the preliminary development of the kinetic model (eq. 1), adsorption of all reactants was considered. However, the initial parameter estimation showed that the calculated terms in the denominator involving adsorption coefficients, for all substances and their concentrations apart from betulonic aldehyde, are very low. This allows assuming that coverage of these species is rather low. The constants in eq. (1) are lumped ones comprising implicitly also dependence on oxygen pressure.

The reactor mass balances for each component in the reaction system are as follows:

$$-\frac{dC_A}{dt} = \rho(r_1 + r_2 + r_5) = \rho \frac{(k_1 + k_2 + k_5)C_A - k_{-5}C_O}{1 + K_D C_D} \quad (2)$$

$$\frac{dC_B}{dt} = \rho(r_2 - r_4) = \rho \frac{k_2 C_A - k_4 C_B}{1 + K_D C_D} \quad (3)$$

$$\frac{dC_C}{dt} = \rho(r_1 - r_3) = \rho \frac{k_1 C_A - k_3 C_C}{1 + K_D C_D} \quad (4)$$

$$\frac{dC_D}{dt} = \rho(r_3 + r_4) = \rho \frac{k_3 C_C - k_4 C_B}{1 + K_D C_D} \quad (5)$$

$$\frac{dC_O}{dt} = \rho(r_5 - r_6) = \rho \frac{k_5 C_A - (k_{-5} + k_6)C_O}{1 + K_D C_D} \quad (6)$$

In eq. (1)-(6) C_i denotes concentration of respective compounds, mol/L, ρ is catalyst bulk density given in g/L. Modified constants, etc. contain also the respective adsorption coefficients.

The differential equations (2-6) were solved using the backward difference method and the parameter estimation was performed with the simplex and Levenberg-Marquardt methods. The numerical tools are inbuilt the optimization software ModEst,⁵⁶ in which the objective function Q is defined through experimental y_i and calculated \hat{y}_i concentrations of the components in the reacting system:



$$Q = \sum (y_i - \hat{y}_i)^2 \quad (7)$$

The results (Fig. 6) show that this model can describe the experimental data rather well.

For 24 data there were initially 8 adjustable parameters, namely 7 rate constants (k_1 to k_6 and k_{-5}) and one adsorption constant (K_D). During the parameter estimation it turned out some of these constants, namely k_3 and k_6 , are negligible. Thus the final model comprised 6 parameters. Their values are given in Table S1. Even is the number of data points is much larger than the number of parameters they were somewhat correlating with each other, preventing a detailed analysis of their physicochemical significance. Apparently, a separate kinetic study accounting for catalyst deactivation and more rigorous chemical analysis of oligomers/polymers is required, being, however, outside of the scope of the current work.

The degree of explanation R^2 :

$$R^2 = 1 - \frac{\sum (y_i - \hat{y}_i)^2}{\sum (y_i - \bar{y})^2} \quad (8)$$

was 99.3% reflecting applicability of the model.

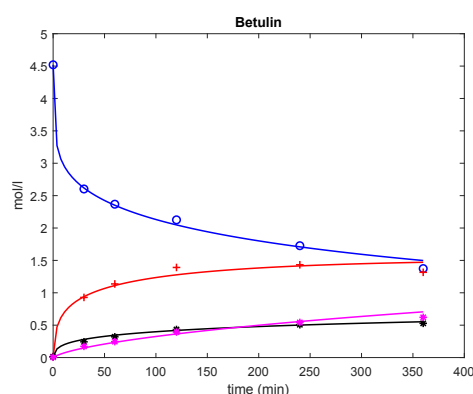


Fig. 6 Comparison between experimental (points) and calculated (lines) concentration profiles in betulin oxidation on Au/La₂O₃/TiO₂_H₂. Conditions and notation of components are given in Fig. 3.

Conclusions

The current work is the first study dealing with the liquid-phase oxidation of betulin over gold-based catalysts. As a support, titania per se, or modified with CeO₂ or La₂O₃, were used. The nature of the support and pretreatment atmosphere (H₂ or O₂) significantly affected the uniformity of gold particles distribution and their mean

size, the electronic state of gold and acid-base properties and, as a consequence, the catalytic behavior (activity and selectivity) of the studied materials in betulin oxidation. The smallest gold nanoparticles with their narrow distribution and the strongest and most stable adsorption sites (Au⁰ and Au⁺) were formed on La-modified TiO₂ surface after H₂ pretreatment. Additionally, this material exhibited the highest basicity and the highest concentration of medium and strong acid sites among the studied catalysts, and as a consequence the best catalytic results. Betulin conversion was 69% for 6 h at 140°C, and the main products were betulone, betulonic and betulinic aldehydes, with selectivities of 42, 32 and 27%, respectively. However, the total yield of products was 1.4 fold lower than the observed conversion, which was due to an incomplete mass balance and was caused by side reactions of oligomerization/polymerization on the catalyst surface, promoted on stronger acid sites. The product yield was increased by adding basic hydrotalcite to the reaction medium along with the catalyst. Such results can be explained by an indirect influence of hydrotalcite on the surface properties of the catalyst, in particular strong acid sites which, in turn prevents the side reactions and increases the product yield. Kinetic modelling was performed to quantify the significance of such side reactions.

Experimental

Catalyst preparation

TiO₂ P25 (nonporous, 70% anatase and 30% rutile, particle size 21 nm, purity 99.5%, Evonik Degussa GmbH) were used as starting support. For comparative studies, titania was modified with ceria and lanthana by impregnation with solutions of the corresponding nitrates (molar ratio Ti/M = 40, where M = Ce or La). After impregnation, the samples were dried at room temperature for 48 h, then at 110°C for 4 h, followed by calcination at 550°C for 4 h.

Gold catalysts (Au/TiO₂, Au/CeO₂/TiO₂ and Au/La₂O₃/TiO₂) were prepared by deposition-precipitation with urea, according to the procedure previously described.^{36,57-59} The nominal gold content in all catalysts was 4 wt.%. The gold precursor (HAuCl₄·3H₂O, Merck) and urea (Merck) were dissolved in distilled water, thereafter the support was added to the solution. The resulting mixture was heated to 80°C and kept at constant temperature for 16 h, with stirring. Thereafter, the catalysts were pretreated at 300°C for 1 hour in H₂ or O₂ atmosphere.

The catalysts are denoted hereinafter as Au/(M_xO_y)/TiO₂_P, where M_xO_y is CeO₂ or La₂O₃ and P indicates the pretreatment atmosphere (O₂ or H₂).

Catalyst characterization

The specific surface area (S_{BET}) of supports and catalysts was measured by nitrogen adsorption with a "TriStar 3000" analyzer (Micromeritics, USA). Prior to measurements, the samples were



subjected to thermal vacuum treatment at 300°C for 5 hours. To calculate the S_{BET} , a multipoint BET method with linearization of the adsorption isotherm for the relative pressure between 0.005 to 0.25 was used.

The phase composition of supports and catalysts was studied by the step-scanning procedure (step size 0.02°; 0.5 s) with Philips XPert PRO diffractometer, using CuK α radiation ($\lambda = 0.15406$ nm) and Ni-filter. The measured diffractograms were analyzed with the ICDD-2013 powder diffraction database.

The morphology of catalysts and the size of gold particles were investigated by transmission electron microscopy (TEM) and STEM-HAADF (scanning transmission electron microscopy-High Angle Annular Dark Field) using a JEOL JEM-2100F. The samples were grounded to a fine powder and sonicated in hexane at room temperature. Then a part of the suspension was placed on a lacey carbon-coated Cu grid. In order to obtain micrographs that most fully reflect the real structure of the samples, a thorough examination of the samples was carried out, after which the selected area was scanned at various resolutions. For each sample, at least 150 particles were registered.

The metal loading of the catalysts was determined by inductively coupled plasma optical emission spectrometry (ICP-OES) Perkin Elmer ICP-OES Optima 3300 DV spectrometer. The solids were dissolved by acid dissolution, digested in a microwave oven, diluted to 100 mL and analyzed in the spectrometer.

The catalysts were characterized by X-ray photoelectron spectroscopy (XPS) with a SPECS GmbH custom made system using a PHOIBOS 150 WAL hemispherical analyzer and a non-monochromated X-ray source. All the data were acquired using Al K α X-rays (1486.6 eV, 200 W). A pass-energy of 50 eV, a step size of 0.1 eV/step and a high-intensity lens mode were selected. The diameter of the analysed area was 3 mm. Charging shifts were referenced against the Ti 2p $_{3/2}$ peak of TiO $_2$ at 458.8 eV. The pressure in the analysis chamber was kept lower than 1×10^{-8} mbar. The accuracy of the binding energy (BE) values was about ± 0.1 eV. Peak areas were estimated by calculating the integral of each peak after subtracting a Shirley type background, fitting the experimental peak to a combination of Lorentzian/Gaussian lines with a 30/70 proportion and keeping the same width on all lines. Deconvolution of spectra was performed with the program CasaXPS.

Diffuse Reflectance Fourier Transform Infrared (DRIFT) spectra of CO adsorbed on the catalysts were recorded by using a Bruker EQUINOX 55/S FTIR spectrometer with homemade accessory at 4 cm $^{-1}$ resolution at room temperature. The powdery fraction of an oxide was placed in a quartz ampoule with a window of CaF $_2$. The samples were preliminarily calcined at 100°C in vacuum not less than 10^{-4} Torr in 1 h. For each catalyst three samples were investigated: as-prepared, and after pretreatments either in H $_2$ or in O $_2$ (100 Torr) at 300°C for 1 h and then cooled down for room temperature. Then, H $_2$ or O $_2$ was evacuated and CO adsorption (>99%) was carried out. The spectra of adsorbed CO were recorded at several pressures — 5, 20, 50 Torr, at room temperature, with the pressure measurement

accuracy of 5%. The obtained spectra were recalculated into Kubelka-Munk units (KMU). The background spectrum was subtracted from the spectrum of the sample with adsorbed CO and the baseline was corrected. All calculations were performed using OPUS 6.0 software (Bruker).

Acidic and basic properties of the catalysts and corresponding supports were studied by temperature-programmable desorption (TPD) of ammonia («Chemosorb» chemical adsorption instrument) and CO $_2$ (Autochem 2900 apparatus), respectively. The procedure in both cases was almost the same apart from the starting desorption temperature, which was 100°C for ammonia TPD and 25°C in the case of CO $_2$ and the carrier gas, in the former case being helium, and the latter argon. Prior to the analysis, the samples were treated at 300°C in the inert atmosphere (helium or argon) for 1 h to remove the impurities adsorbed on the surface. Thereafter, the temperature was decreased to 100°C (25°C) followed by saturation with NH $_3$ (CO $_2$) for 60 min and flushing with He (Ar) for 1 h to remove physisorbed NH $_3$ (CO $_2$). The temperature was increased to 600°C with 10°C/min ramp in helium (argon) atmosphere.

For comparative analysis, NH $_3$ and CO $_2$ desorption profiles of the supports and corresponding catalysts are demarcated into temperature ranges: 100 – 200°C (for TPD CO $_2$ starting temperature 25°C), 200 – 400°C and 400 – 600°C and are designated as weak, medium and strong acid or basic sites, respectively.

Catalytic testing

Betulin (90-94%) was extracted from birch with a non-polar solvent and recrystallized from 2-propanol in Åbo Akademi University.² Betulin oxidation was performed over supported Au catalysts under atmospheric pressure with synthetic air (AGA, 20% oxygen, 80% nitrogen) as an oxidant in mesitylene at 140°C or in toluene at 108 °C (Sigma Aldrich, > 99%). Synthetic air was bubbled through the liquid with the inlet for the gas (flow rate 50 ml/min) located at the bottom of the reactor to enhance the gas-liquid mass transfer. Moreover, a metallic sinter was applied to diminish the size of air bubbles. Typically oxidation of betulin was carried out using 200 mg of the reagent in 100 ml of the solvent (the initial betulin concentration was 4.5 mmol/l) using 200 mg of the catalyst. The reaction started when the desired temperature was reached, via turning on the stirring (450 rpm). Small catalyst particles (< 63 μ m) and high stirring rate of 450 rpm were used to suppress the internal and external mass transfer limitations. In some experiments, hydrotalcite (Merck) was used together with the catalyst as a base-additive. Hydrotalcite was calcined for 3 h at 500°C prior to its use.

The samples for analysis were withdrawn from the reactor at regular intervals. Prior to GC-analyses, the samples (150 μ L) were silylated by adding 150 μ L of a mixture of pyridine (VWR International, Fontenay-sous-Bois, France), N,O-bis(trimethylsilyl)trifluoroacetamide (BSTFA, Supelco Analytical, Bellefonte, PA, USA), and trimethylsilyl chloride (TMCS, Merck KGaA, Darmstadt, Germany) in a 1:4:1 volume ratio, and the mixture was



heated in an oven at 70°C for 45 min. GC analysis was performed on a PerkinElmer AutosystemXL gas chromatograph using an Agilent HP-1 capillary column, 25 m (L) × 0.2 mm (ID), film thickness 0.11 mm. Hydrogen was used as a carrier gas, with a flow of 0.8 ml/min. Betulinic aldehyde and betulinic acid (90% purity), used as standards, were purchased from MedChem Express and Merck, respectively. The products were confirmed by GC-MS. The conditions of betulin oxidation and the analytical procedure were previously published.^{34,35}

Size exclusion chromatography was performed to investigate oligomers and polymers formation on the spent catalysts surface.⁶⁰ 20 mg of the spent catalysts was added to a round flask together with 20 ml of the solvent heptane and a condenser. The flask was placed in an oil bath and heated to 98°C. Thereafter, extraction occurred for four hours with a stirring rate of 400 rpm. The flowrate of the inert gas, consisting of 5 % Ar in 95 % N₂, was set to 100 ml/min. The solution obtained after the 4 h extraction was then kept at 40°C, until complete evaporation of heptane. The resulting residue was then dissolved in 10 ml of tetrahydrofuran, being thereafter filtered for analysis. The resulting concentration of the residue was 2 mg/ml. The analysis was carried out using a SEC-HPLC equipped with two columns, a Guard column with the dimensions of 50 mm × 7.8 mm and a Jordi Gel DVB 500A column with the dimensions of 300 mm × 7.8 mm.

The TOF values were calculated as the number of converted moles of betulin per mole of exposed catalytic site per unit time, during the first 15 min, taking into account the metal dispersion:

$$TOF = \frac{n_{Betulin}}{n_{Metal}Dt} \quad (9)$$

where $n_{Betulin}$ is number of converted moles of betulin, n_{Metal} is the number of moles of the metal, D is dispersion and t is time. The number of surface metal atoms was calculated knowing the average gold particle size measured by transmission electron microscopy (TEM).

Conflicts of interest

There are no conflicts to declare.

Acknowledgements

The research is funded from the Russian Science Foundation project № 18-73-00019 and Tomsk Polytechnic University Competitiveness Enhancement Program, project VIU-ISHBMT-65/2019 (Russia). SACC acknowledges Fundação para a Ciência e a Tecnologia (FCT) for Investigador FCT program (IF/01381/2013/CP1160/CT0007). This work was also financially supported by Associate Laboratory LSRE-LCM - UID/EQU/50020/2019 - funded by national (Portuguese) funds through FCT/MCTES (PIDDAC).

References

- [1] E. W. H. Hayek, U. Jordis, W. Moche, F. Sauter, *Phytochem.* **1989**, 28, 2229.
- [2] C. Eckerman, R. Ekman, *Paperi ja Puu* **1985**, 67, 100.
- [3] H. Pakdel, M. Murwanashyuka, C. Roy, *J. Wood Chem. Technol.* **2002**, 22, 147.
- [4] S. Ohara, Y. Hayashi, M. Yatagai, *Henkan Keikaku Kenkyu Hokoku* **1990**, 24, 12. [C. A. 120 (1994) 301339f].
- [5] B.N. Kuznetsov, V.A. Levdansky, N.I. Polezhaeva, *Chem. Plant Raw Mater.* **2004**, 2, 21 - 24.
- [6] G. A. Tolstikov, O. B. Flekhter, E. E. Shultz, L. A. Baltina, A. G. Tolstikov, *Chem. Sus. Dev.* **2005**, 13, 1–29.
- [7] S. Alakurtti, T. Mäkelä, S. Koskimies, *Eur. J. Pharm. Sci.* **2006**, 29, 1–13.
- [8] R.C. Santos, J.A.R. Salvador, S. Marín, *Bioorg&Med. Chem.* **2009**, 17, 6241-6250.
- [9] S.C. Jonnalagadda, P. Suman, D.C. Morgan, J.N. Seay, *Stud. Nat. Prod. Chem.* **2004**, 53, 45-84.
- [10] V. V. Grishko, E. V. Tarasova, I. B. Ivshina, *Proc. Biochem.* **2013**, 48, 164-1644.
- [11] S. Alakurtti, P. Bergström, N. Sacerdoti-Sierra, C.L. Jaffe, *J. Yli-Kauhaluoma, J. Antibiot.* **2010**, 63, 123-126.
- [12] M.S Gachet, O. Kunert, M. Kaiser, R. Brun, M. Zehl, W. Keller, R.A. Munoz, R. Bauer, W. Schuehly, *J. Nat. Prod.* **2011**, 74, 559-566.
- [13] C.P. Reyes, M.J. Núñez, I.A. Jiménez, J. Busserolles, M.J. Alcaraz, L. Bazzocchil, *Bioorg. Med. Chem.* **2006**, 14, 1573-1579.
- [14] K. Hata, K. Hori, S. Takahashi, *J. Nat. Prod.* **2002**, 65, 645-648.
- [15] A. Koohang, N.D. Majewski, E.L. Szotek, A.A. Mar, D.A. Eiznhamer, M.T. Flavin, Z.Q. Xu, *Bioorg. Med. Chem. Lett.* **2009**, 19, 2168-2171.
- [16] M. Liu, S. Yang, L. Jin, D. Hu, Z. Wu, S. Yang, *Molecules* **2012**, 17, 6156–6169.
- [17] A.A. Mar, A. Koohang, N.D. Majewski, E.L. Szotek, D.A. Eiznhamer, M.T. Flavin, Z.Q. Xu, *Chin. Chem. Lett.* **2009**, 20, 1141-1141.
- [18] I.C. Sun, J.K. Shen, H.K. Wang, L.M. Cosentino, K.H. Lee, *Bioorg. Med. Chem. Lett.* **1998**, 8, 1267-1272.
- [19] I.C. Sun, H.K. Wang, Y. Kashiwada, J.K. Shen, L.M. Cosentino, C.H. Chen, L.M. Yang, K.H. Lee, *J. Med. Chem.* **1998**, 41, 4648-4657.
- [20] E. Bębenek, M. Kadela-Tomanek, E. Chrobak, J. Wietrzyk, J. Sadowska, S. Boryczka, *Med. Chem. Res.* **2016**, 26, 1–8.
- [21] E. Bębenek, M. Kadela-Tomanek, E. Chrobak, M. Latocha, S. Boryczka1, *Med. Chem. Res.* **2018**, 27, 2051-2061.
- [22] V.V. Grishko, I. A. Tolmacheva, V.O. Nebogatikov, N.V. Galaiko, A.V. Nazarov, M.V. Dmitriev, I.B. Ivshina, *Eur. J. Med. Chem.* **2017**, 125, 629-639.
- [23] R. Csuk, K. Schmuck, R. Schafer, *Tetrahedron Lett.* **2006**, 47, 8769-8770.

View Article Online

DOI: 10.1039/C9GC00949C



- [24] A. Pichette, H. Liu, C. Roy, S. Tanguay, F. Simard, S. Lavoie, *Synth. Commun.* **2004**, *34*, 3925–3937.
- [25] N. G. Komissarova, N. G. Belenkova, O.V. Shitikova, L. V. Spirikhin, M. S. Yunusov, *Chem. Nat. Compd.* **2006**, *338*(1), 58–61.
- [26] S. D. Kim, Z. Chen, T. V. Nguyen, J. M. Pezzuto, S. Qui, Z. Z. Lu, *Synth. Commun.* **1997**, *27*, 1607–1612.
- [27] J. M. Pezzuto, S. H. L. Darrick Kim, Pat US 5804575, **1998**.
- [28] V. I. Roshchin, N. Yu. Shabanova., D. N. Vedernikov, Pat RU 2190622, **2002** [MGG C07J053/00, C07J063/00].
- [29] V. A. Levdansky, N. I. Polezhaeva, B. N. Kuznetsov, Pat RU 2269541 **2004** [IPC C07J53/00, C07J63/00].
- [30] K. Muffler, D. Leipold, M. Schellera, C. Haas, J. Steingroewer, T. Bley, H. E. Neuhaus, M. A. Mirata, J. Schrader, R. Ulber, *Proc. Biochem.* **2011**, *46*, 1–15.
- [31] D.B. Mao, Y.Q. Feng, Y.H. Bai, C.P. Xu, *J. Taiwan Inst. Chem. Eng.* **2012**, *43*, 825–829.
- [32] H. Liu, X.L. Lei, N. Li, M.H. Zong, *J. Mol. Catal. B: Enzym.* **2013**, *88*, 32–35.
- [33] E. V. Tarasova, V.V. Grishko, I. B. Ivshina, *Proc. Biochem.* **2017**, *52*, 1–9.
- [34] P. Mäki-Arvela, M. Barsukova, I. Winberg, A. Smeds, J. Hemming, K. Eränen, A. Torozova, A. Aho, K. Volcho, D. Yu. Murzin, *Chem. Select.* **2016**, *1*, 3866–73869.
- [35] E. Kolobova, Y. Kotolevich, E. Pakrieva, G. Mamontov, M.H. Farias, V. Cortés Corberán, N. Bogdanchikova, J. Hemming, A. Smeds, P. Mäki-Arvela, D. Yu. Murzin, A. Pestryakov, *Fuel* **2018**, *234*, 110–119.
- [36] R. Zanella, L. Delannoy, C. Louis, *Appl. Catal. A: Gen.* **2005**, *29*, 62–72.
- [37] E. Pakrieva, E. Kolobova, G. Mamontov, N. Bogdanchikova, M. H. Farias, L. Pascual, V. Cortés Corberán, S. Martinez Gonzalez, S. A. C. Carabineiro, A. Pestryakov, *ChemCatChem* **2019**, *11*, 1–11.
- [38] A. Penkova, K. Chakarova, O. H. Laguna, K. Hadjiivanov, F. Romero Saria, M. A. Centeno, J. A. Odriozola, *Catal. Commun.* **2009**, *10*, 1196–1202.
- [39] A. N. Pestryakov, A. A. Davydov, *Appl. Catal. A* **1994**, *120*, 7–15.
- [40] Y. Kotolevich, E. Kolobova, E. Khramov, M.H. Farías, Ya. Zubavichus, H. Tiznado, S. Martínez-González, V. Cortés Corberán, J.D. Mota-Morales, A. Pestryakov, N. Bogdanchikova, *J. Mol. Cat. A: Chem.* **2017**, *427*, 1–10.
- [41] A. Simakov, I. Tuzovskaya, A. Pestryakov, N. Bogdanchikova, V. Gurin, M. Avalos, M.H. Farias., *App. Catal. A: Gen.* **2007**, *331*, 121–128.
- [42] N. Bogdanchikova, A. Pestryakov, I. Tuzovskaya, T.A. Zepeda, M. H. Farias, H. Tiznado, O. Martynyuk, *Fuel* **2013**, *110*, 40–47.
- [43] S. V. Nayak, R. V. Chodhary, *J Catal.* **1983**, *81*(1), 26–45.
- [44] H. D. Olson, T. G. Kokotailo, L. S. Lawton, M. W. Meier, *J. Phys. Chem.* **1981**, *85*(15), 2238–43.
- [45] L. Zhu, Y. Zeng, Sh. Zhang, J. Deng, Q. Zhong, *J. Env. Sci.* **2017**, *54*, 277–287. DOI: 10.1039/C9GC00949C
- [46] P.N. Amaniampong, K. Li, X. Jia, B. Wang, A. Borgna, Y. Yang, *ChemCatChem.* **2014**, *6*, 2105 – 2114.
- [47] D. Kubicka, N. Kumar, P. Mäki-Arvela, M. Tiitta, V. Niemi, H. Karhu, T. Salmi, D.Yu. Murzin, *J. Catal.* **2004**, *227*, 313–327.
- [48] D. Kubicka, N. Kumar, T. Venäläinen, H. Karhu, I. Kubickova, H. Österholm, D.Yu. Murzin, *J. Phys. Chem. B* **2006**, *110*, 4937–4946.
- [49] J. I. Villegas, D. Kubicka, H. Karhu, H. Österholm, N. Kumar, T. Salmi, D. Yu. Murzin, *J. Mol. Catal. A. Chem.* **2007**, *264*, 192–201.
- [50] D. N. Thanh, O. Kikhtyanin, R. Ramos, M. Kothari, P. Ulbrich, T. Munshi, D. Kubicka, *Catal. Today* **2016**, *277*, 97–107.
- [51] J. I. Di Cosimo, V. K. Diez, M. Xu, E. Iglesia, C. R. Apesteguia, *J. Cat.* **1998**, *178*, 499–510.
- [52] M. Di Serio, M. Ledda, M. Cozzolino, G. Minutillo, R. Tesser, E. Santacesaria, *Ind. Eng. Chem. Res.* **2006**, *45*, 3009–3014.
- [53] C. O. Veloso, C. N. Pérez, B. M. de Souza, E. C. Lima, A. G. Dias, J. L. F. Monteiro, C. A. Henriques, *Micr. Mes. Mater.* **2008**, *107*, 23–30.
- [54] M. Mihaylov, E. Ivanova, Y. Hao, K. Hadjiivanov, B. C. Gates, H. Knozinger, *Chem. Commun.* **2008**, 175–177.
- [55] M. Mihaylov, E. Ivanova, Y. Hao, K. Hadjiivanov, H. Knozinger, B. C. Gates, *J. Phys. Chem. C* **2008**, *112*, 18973–189.
- [56] H. Haario, ModEst, Modelling and optimization software, Helsinki (Finland), **2011**.
- [57] R. Zanella, S. Giorgio, C. R. Henry, C. Louis, *J. Phys. Chem. B* **2002**, *106*, 7634–7642.
- [58] M. Hinojosa-Reyes, R. Camposeco-Solis, R. Zanella, V. Rodríguez-González, F. Ruiz, *Catal. Lett.* **2018**, *148*(1), 383–396.
- [59] R. Zanella, C. Louis, *Catal. Today* **2005**, 107–108, 768–777.
- [60] A. H. Abdullah, A. Hauser, F. A. Ali, A. Al-Adwani, *Energy Fuels* **2006**, *20*(1), 320–323.

